

Comparison of frequency-domain and time-domain fluorescence lifetime tomography

Anand T. N. Kumar,^{1,*} Scott B. Raymond,² Brian J. Bacskaï,³ and David A. Boas¹

¹Athinoula A. Martinos Center for Biomedical Imaging, Massachusetts General Hospital, Harvard Medical School, Charlestown, Massachusetts 02129, USA

²Harvard-MIT Division of Health Sciences and Technology, Boston, Massachusetts 02115, USA

³Alzheimer's Disease Research Unit, Department of Neurology, Massachusetts General Hospital, Charlestown, Massachusetts 02129, USA

*Corresponding author: ankumar@nmr.mgh.harvard.edu

Received December 4, 2007; revised January 17, 2008; accepted January 22, 2008;
posted January 30, 2008 (Doc. ID 90394); published February 25, 2008

We compare frequency- and time-domain formulations of deep-tissue fluorescence imaging of turbid media. Simulations are used to show that time-domain fluorescence tomography, implemented via the asymptotic lifetime-based approach, offers a significantly better separability of multiple lifetime targets than a frequency-domain approach. We also demonstrate experimentally, using complex-shaped phantoms, the advantages of the asymptotic time-domain approach over a Fourier-based approach for analyzing time-domain fluorescence data. © 2008 Optical Society of America
OCIS codes: 170.3880, 170.3650.

Optical technologies for noninvasive macroscopic fluorescence imaging in biological media utilize three main approaches: time domain (TD) using pulsed light sources [1–5], frequency domain (FD) using megahertz modulated sources [6–8], and continuous wave (CW) using steady state light sources [9–11]. Of these, the TD approach is the most comprehensive, since a short laser pulse (fs-ps) implicitly contains all the modulation frequencies, including the zero-frequency component. The tomographic analysis of TD data can, however, pose computational challenges. Several simplifications have been attempted, primarily using derived data types such as the fast Fourier transform (FFT) [5,7]. The FFT simplifies the TD forward problem but reduces it to a FD forward problem, identical to that for a genuine FD measurement. Alternatively, TD fluorescence data may also be analyzed by estimating lifetimes directly from the asymptotic region, followed by the separate inversion of the yield of each lifetime component [3,12]. The question arises as to how the FD forward problem compares with the asymptotic TD (ATD) approach, when lifetime sensitive targets are used. In this Letter, we address this question both with simulated and experimental TD data in the context of small animal imaging applications.

Consider a diffuse imaging medium of finite support Ω , embedded with fluorophores characterized by yield and lifetime distributions, $\eta(\mathbf{r})$ and $\tau(\mathbf{r})$. In the FD approach, the forward problem takes the form [6]

$$\tilde{U}(\mathbf{r}_s, \mathbf{r}_d, \omega) = \int_{\Omega} d^3r G^x(\mathbf{r}_s, \mathbf{r}, \omega) G^m(\mathbf{r}_d, \mathbf{r}, \omega) F(\mathbf{r}, \omega). \quad (1)$$

Here, G^x and G^m are the FD Green's functions at frequency ω for propagation from a source \mathbf{r}_s and a detector \mathbf{r}_d , respectively, to a medium point \mathbf{r} . Equation (1) is first inverted to obtain $F(\mathbf{r}, \omega) = \tau(\mathbf{r})\eta(\mathbf{r})/[1 - i\omega\tau(\mathbf{r})]$. The lifetimes are then obtained from the phase $\phi(\mathbf{r}, \omega)$ of F , as $\tau(\mathbf{r}) = \phi(\mathbf{r}, \omega)/\omega$. Finally, the

yield reconstructions are given by $\eta(\mathbf{r}) = \Re e[F](1 + \omega^2\tau(\mathbf{r})^2)/\tau(\mathbf{r})$. In the ATD approach, the decay amplitudes, $a_n(\mathbf{r}_s, \mathbf{r}_d)$, for each lifetime component, $\tau_n = 1/\Gamma_n$, take the place of the Fourier amplitude, \tilde{U} , as the measurement data set [3]. The a_n 's are related to the yield distribution, $\eta_n(\mathbf{r})$, for the lifetime component at τ_n , through a linear forward problem:

$$a_n(\mathbf{r}_d, \mathbf{r}_s) = \int_{\Omega} d^3r G^x(\mathbf{r}_s, \mathbf{r}, -i\Gamma_n) G^m(\mathbf{r}_d, \mathbf{r}, -i\Gamma_n) \eta_n(\mathbf{r}). \quad (2)$$

Note that in Eq. (2), the Green's functions are the same as that for the FD case in Eq. (1), but evaluated at an imaginary frequency of $-i\Gamma_n$. (see [12] for details). The difference between Eq. (1) and Eq. (2) is clear if we express $F(\mathbf{r}, \omega)$ in terms of discrete lifetimes rather than the continuous distributions $\tau(\mathbf{r})$. We then get $F(\mathbf{r}, \omega) = \sum_n \tau_n \eta_n(\mathbf{r}) / (1 - i\omega\tau_n)$. Thus the FD approach recovers a single distribution, $F(\mathbf{r}, \omega)$, that is a mixture of the yields for all the lifetimes present in the imaging medium. Separability of multiple lifetime components using the FD approach will therefore be limited by the intrinsic resolution of the system. The ATD approach, however, results in a separate forward problem for each lifetime, so that only the widths of the individual $\eta_n(\mathbf{r})$'s are subject to the resolution limitations. The spatial separability of the η_n 's for different lifetimes in the ATD approach relies rather on the ability to recover the lifetimes through multiexponential fits of TD decays.

To compare the performance of the FD and ATD approaches, simulations were performed for a 2 cm thick infinite slab geometry, assuming 2 mm \times 2 mm \times 2 mm size fluorescent targets (also the size of a single voxel) placed both laterally (Fig. 1) and axially (Fig. 2) with respect to the source-detector line of sight. The inclusions had distinct lifetimes of 0.5 and 1 ns. 29 sources and 21 detectors were arranged [Fig. 1(a)] along the planes at depths of $z=0$ cm and

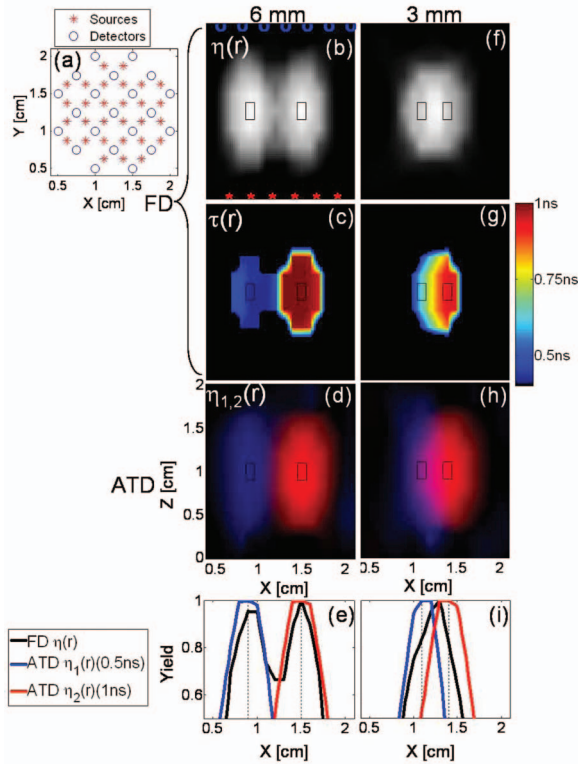


Fig. 1. Comparison of FD and ATD reconstructions with simulated data for laterally located fluorescent targets with lifetimes of 0.5 and 1 ns. (a) Cross-sectional (x - y plane) view of sources (asterisks) and detectors (circles) arranged in a transmission geometry for a 2 cm thick infinite slab. Sources were in the $z=0$ cm plane, and detectors were in the $z=2$ cm plane. The FD reconstructed $\eta(\mathbf{r})$ and $\tau(\mathbf{r})$ are shown for 6 mm separated targets in (b) and (c), and for 3 mm separated targets in (f) and (g). The $\tau(\mathbf{r})$ images are displayed only in the region within 50% of the maximum of $\eta(\mathbf{r})$. The ATD reconstructed yields are shown in (d) for 6 mm separation and (h) for 3 mm separation. The images in (d) and (h) are displayed by assigning the yield for 0.5 ns to the blue component and that for 1 ns to the red component of a single RGB image. [As a visual aid, the color scales in (c) and (g) are also restricted to a range of 0.5 ns (blue) to 1 ns (red).] (e) and (i) show plots of normalized yield along the x direction at the (y,z) location of the maxima of the corresponding $\eta(\mathbf{r})$'s. (see legend). The vertical dotted lines indicate the true centroids of the inclusions.

$z=2$ cm, respectively. The background medium was assumed to have values of $\mu'_s=10$ cm $^{-1}$ for scattering and $\mu_a=0.1$ cm $^{-1}$ for absorption (at both excitation and emission wavelengths). The FD signal was simulated using Eq. (1) in the diffusion approximation, for $\omega=80$ MHz, and reconstructed with Tikhonov regularization. The full TD signal was also simulated in the diffusion model with shot noise added, and the $a_n(\mathbf{r}_s, \mathbf{r}_d)$'s were recovered asymptotically. Figures 1(b) and 1(c) show the FD recovered $\eta(\mathbf{r})$ and $\tau(\mathbf{r})$, and Fig. 1(d) shows the ATD recovered $\eta(\mathbf{r})$ for 0.5 and 1 ns, for a lateral target separation of 6 mm. Figures 1(f)–1(h) show the corresponding images for 3 mm separation. The x dependence of the yield for each case is plotted at the (y,z) location of the maximum of the corresponding distributions in Figs. 1(e)

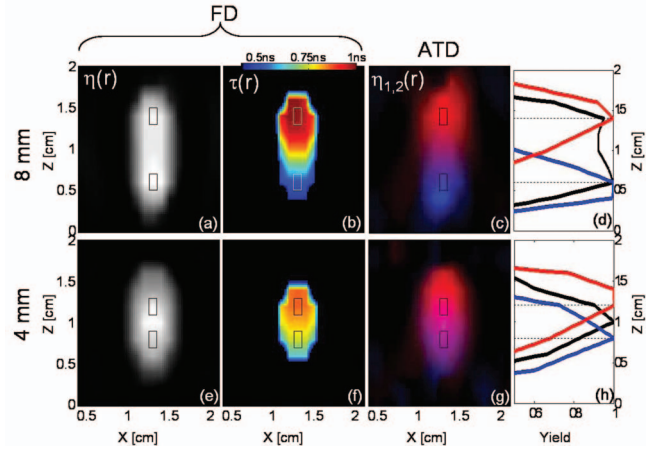


Fig. 2. Comparison of FD and ATD reconstructions for axially targets. The geometry is the same as in Fig. 1. The FD reconstructed $\eta(\mathbf{r})$ and $\tau(\mathbf{r})$ are shown for 8 mm separated targets in (a) and (b), and for 4 mm separated targets in (e) and (f). The ATD reconstructed yields are shown in (c) for 8 mm separation and (g) for 4 mm separation. (d) and (h) show the z dependence of the yields at the x - y location of the individual maxima. The dotted lines indicate the true centroids of the inclusions. The color scheme is identical to that of Fig. 1.

and 1(i). It is clear that while the ATD approach localizes and resolves the targets for both separations, the FD approach does not clearly resolve the targets for the 3 mm case [Figs. 1(f) and 1(i)] and results in an inaccurate lifetime estimate [Fig. 1(g)]. Also, $\tau(\mathbf{r})$ exhibits a continuous variation in the region between the targets [Fig. 1(g)]. Figure 2 shows the results when targets are located axially, i.e., along the normal to the source and detector planes. The ATD approach resolves the targets for both an 8 and a 4 mm separation as seen from Figs. 2(d) and 2(h). For the 8 mm separation, the FD approach barely resolves the targets, but $\tau(\mathbf{r})$ is obtained accurately near the target locations. However, $\tau(\mathbf{r})$ again varies continuously between 0.5 and 1 ns in the region between the targets [Fig. 2(b)]. Thus a continuous distribution of lifetimes is recovered by the FD approach for both axial and lateral targets, although discrete lifetimes were simulated. The FD approach completely fails to recover the targets for the 4 mm separation [Fig. 2(h), black curve] and recovers an inaccurate lifetime distribution [Fig. 2(f)]. We also independently verified that using multiple frequencies does not significantly improve the quality of the FD reconstructions. Specifically, the 3 mm separated lateral targets in Fig. 1 and 4 mm axial targets in Fig 2 were not resolved with the use of up to 5 frequencies, even using a simplified linear approach where the lifetimes were assumed to be known in advance. (Multifrequency FD is a nonlinear problem [7].)

The simulations presented in Figs 1 and 2 clearly indicate the advantages of the ATD approach over the FD formalism for resolving lifetime contrast. We now experimentally demonstrate these results using a noncontact TD fluorescence tomography system, consisting of a Ti:Sapphire laser source for excitation and a time-gated intensified CCD camera for detec-

tion. Detailed aspects of the system are discussed in a separate publication [4]. A mouse-shaped phantom made of epoxy, ink, and TiO₂ combination ($\mu'_s = 10 \text{ cm}^{-1}$, $\mu_a = 0.1 \text{ cm}^{-1}$) was used as the imaging subject [Fig. 3(a)]. Two inclusions ($\approx 3 \text{ mm} \times 3 \text{ mm} \times 3 \text{ mm}$ in size, 6 mm center-to-center separation) within the phantom were filled with a near-infrared dye (3,3'-diethylthiatricarbocyanine, absorption and emission maxima near 755 and 790 nm), mixed in distilled water and 100% glycerol solutions, giving lifetimes of 0.5 and 0.95 ns. The data were collected in the transillumination geometry for 21 source positions (1 mm \times 1 mm grid) and 33 assigned detectors (1 mm \times 2 mm grid) on the CCD camera image. The lifetimes were directly recovered from a global analysis fit [4] to the experimental decay curves as near 0.5 and 0.95 ns, and the decay amplitudes at all the S-D pairs were used in Eq. (2) to recover the yield. The 3D reconstructions of the yield of the two lifetimes recovered using the ATD approach are shown in Fig. 3(b), overlaid with the surface boundary of the phantom, which was acquired using photogrammetric methods [11]. The first Fourier component of the data, at 156 Mhz, was also used in a FD approach using Eq. (1). Reconstructions were performed for

data with both one lifetime (single inclusion filled) and two lifetimes (both inclusions filled). It is clear from the tomography results of Figs. 3(c)–3(j) that the ATD approach recovers the target depths for both the single and two lifetime cases. While the FD approach recovers the correct localization and lifetime for the single lifetime case, it does not localize the targets separately when both inclusions are simultaneously filled and estimates an inaccurate lifetime of $\approx 0.7 \text{ ns}$. It should be noted again that, as seen in the simulations, the ATD approach is able to separate targets located well within the full width at half-maximum of the yield for a single inclusion, which was $> 1 \text{ cm}$ [Fig. 3(f)].

We have shown using simulations and experiments that an asymptotic multiexponential-analysis-based TD approach to fluorescence tomography has inherent advantages over the FD formalism of diffuse fluorescence when resolving discrete lifetimes present within a turbid medium. Fluorescence lifetime has been widely exploited in microscopy techniques with thin tissue sections (see, for example, [13]), and it is likely to serve as a key functional parameter for non-invasive diagnostic optical molecular imaging and drug discovery. The findings reported in this Letter have significant relevance for the design of lifetime-based optical molecular imaging systems. The results also strongly motivate further development of smart near-infrared molecular probes that specifically shift lifetime upon binding to disease targets of interest.

This work was supported by the National Institutes of Health (grants EB000768 and AG026240).

References

1. J. Wu, L. Perelman, R. R. Dasari, and M. S. Feld, Proc. Natl. Acad. Sci. U.S.A. **94**, 8783 (1997).
2. S. Bloch, F. Lesage, L. Mackintosh, A. Gandjbakche, K. Liang, and S. Achilefu, J. Biomed. Opt. **10**, 054003-1 (2005).
3. A. T. N. Kumar, J. Skoch, B. J. Bacskai, D. A. Boas, and A. K. Dunn, Opt. Lett. **30**, 3347 (2005).
4. A. T. N. Kumar, S. B. Raymond, A. K. Dunn, B. J. Bacskai, and D. A. Boas, "A time domain fluorescence tomography system for small animal imaging," IEEE Trans. Med. Imaging (to be published).
5. V. Y. Soloviev, J. McGinty, K. B. Tahir, M. A. A. Neil, A. Sardini, J. V. Hajnal, S. R. Arridge, and P. M. W. French, Opt. Lett. **32**, 2034 (2007).
6. M. A. O'Leary, D. A. Boas, X. D. Li, B. Chance, and A. G. Yodh, Opt. Lett. **21**, 158 (1996).
7. A. B. Milstein, J. J. Stott, S. Oh, D. A. Boas, R. P. Millane, C. A. Bouman, and K. J. Webb, J. Opt. Soc. Am. A **21**, 1035 (2004).
8. A. Godavarty, E. M. Sevick-Muraca, and M. J. Eppstein, Med. Phys. **32**, 992 (2005).
9. V. Ntziachristos and R. Weissleder, Opt. Lett. **26**, 893 (2001).
10. E. E. Graves, J. Ripoll, R. Weissleder, and V. Ntziachristos, Med. Phys. **30**, 901 (2003).
11. R. B. Schultz, J. Ripoll, and V. Ntziachristos, IEEE Trans. Med. Imaging **23**, 492 (2004).
12. A. T. N. Kumar, S. B. Raymond, G. Boverman, D. A. Boas, and B. J. Bacskai, Opt. Express **14**, 12255 (2006).
13. P. I. H. Bastiaens and A. Squire, Trends Cell Biol. **9**, 48 (1999).

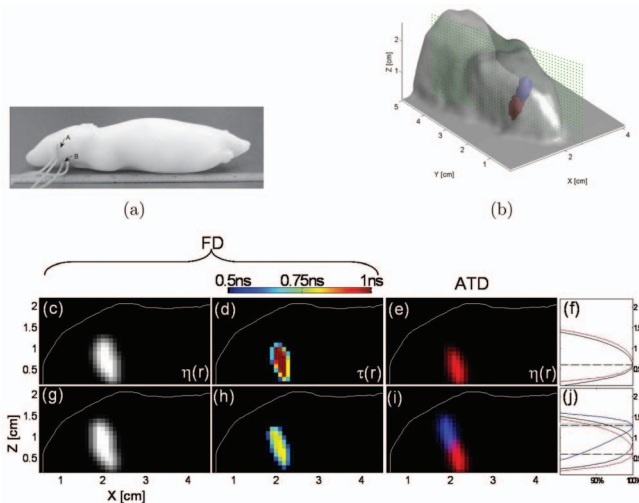


Fig. 3. Experimental tomography results from a mouse phantom. (a) Photograph of mouse phantom used, with two inclusions. Inclusion A was filled with an aqueous solution of the fluorophore (0.5 ns lifetime), and inclusion B was filled with the fluorophore in 100% glycerol (0.95 ns lifetime). (b) ATD reconstructions are shown as 90% isosurfaces (yield for 0.5 ns in blue and yield for 0.95 ns in red) overlaid with the surface boundary of the phantom obtained using a 3D camera system. (c–j) show both the ATD and FD reconstructions along the planar slice (green dots) shown in (b). (c–f) Reconstructions with only B filled with the dye solution in glycerol. (g–j) Reconstructions with both A and B filled with the aqueous and glycerol dye solutions, respectively. (c) and (g) show $\eta(\mathbf{r})$, and (d) and (h) show $\tau(\mathbf{r})$ recovered using the 156 Mhz Fourier component of the TD data. (e, i) ATD yield displayed as an RGB image, with blue and red components assigned the yields for 0.5 and 0.95 ns, respectively. All the yields are thresholded at 90% of the maximum. (f) and (j) are the depth (z) profiles of all the yields at the (x, y) location of the corresponding maximum yield. The color scheme is identical to that of Fig. 1.